RSC Advances

This is an *Accepted Manuscript*, which has been through the Royal Society of Chemistry peer review process and has been accepted for publication.

Accepted Manuscripts are published online shortly after acceptance, before technical editing, formatting and proof reading. Using this free service, authors can make their results available to the community, in citable form, before we publish the edited article. This *Accepted Manuscript* will be replaced by the edited, formatted and paginated article as soon as this is available.

You can find more information about *Accepted Manuscripts* in the Information for Authors.

Please note that technical editing may introduce minor changes to the text and/or graphics, which may alter content. The journal's standard Terms & Conditions and the Ethical guidelines still apply. In no event shall the Royal Society of Chemistry be held responsible for any errors or omissions in this *Accepted Manuscript* or any consequences arising from the use of any information it contains.

ROYAL SOCIETY OF CHEMISTRY

www.rsc.org/advances

Composition-Dependent Structural and Electrical Properties of P-type SnO_x Thin Films Prepared by Reactive DC Magnetron Sputtering: Effects of Oxygen Pressure and Heat Treatment

Sang Jin Han[1], Sungmin Kim[1], Joongyu Ahn[3], Jae Kyeong Jeong[2,], Hoichang Yang[3,#], and Hyeong Joon Kim[1,$]*

[1]Department of Materials Science and Engineering, and Inter-university Semiconductor Research Center, Seoul National University, Seoul 151-742, Republic of Korea

[2]Department of Electronic Engineering, Hanyang University, Seoul 133-791, Republic of Korea

[3]Department of Applied Organic Materials Engineering, Inha University, Incheon 402-751, Republic of Korea

KEYWORDS: tin oxide; p-type semiconductor; thin film transistor; oxygen pressure; heat treatment temperature.

RSC Advances Accepted Manuscript

ABSTRACT

The composition-dependent structural and electrical properties of SnO_x films prepared by means of reactive DC sputtering at various oxygen partial pressure (P_O) and post-heat treatment temperature (T_A) were investigated, toward these films' potential use in p-channel oxide thin-film transistors (TFTs). A SnO_x film fabricated under the lowest studied P_O of 4 % and heat-treated at 210 °C consisted of dendritic phases and irregular protrusions of metallic Sn. The resulting p-channel SnO_x thin-film transistors suffered from marginal field effect mobility (μ_{FE}) and low on/off current ratio ($I_{ON/OFF}$), suggesting that the imperfect phases caused by oxygen-deficient stoichiometry hinder hole carrier conduction and act as bulk trap states. The heterogeneous structures observed in SnO_x films annealed at 210 °C could be eliminated by increasing P_O during fabrication. The resulting TFTs based on p-type SnO_x films prepared at the high P_O of 8 % showed high mobilities up to 2.8 cm^2 V^{-1} s^{-1} and reasonable $I_{ON/OFF}$ of approximately 10^3, demonstrating the critical role of these films' homogeneous ordered aggregates without any imperfect phases such as dendritic phase or irregular protrusions of metallic Sn. Among TFTs based on the films fabricated under 8 % P_O, the μ_{FE} and $I_{ON/OFF}$ performance metrics degraded with increasing T_A from 210 to 300 °C, which was mainly related to the $2SnO \rightarrow SnO_2 + Sn$ disproportionation reaction.

RSC Advances Accepted Manuscript

1. Introduction

Metal oxide semiconductors (MOSs) have received remarkable attention as backplane materials for flat panel displays such as those based on liquid crystals (LCs) and organic light emitting diodes (OLEDs), due to their cost-effective, low-temperature processability and high carrier mobility. Recently, MOSs have been studied extensively as candidate materials for emerging applications such as flexible and transparent electronics, owing to their outstanding characteristics including high optical transparency and electrical conductivity.[1-3]

N-type InGaZnO-based TFTs have been commercialized as backplane components of flat panel displays, yielding electron mobilities over 10 $cm^2\ V^{-1}\ s^{-1}$.[4] However, p-type MOSs still need to be improved. This discrepancy between types arises mainly from the difference in their band structures: in n-type oxide semiconductors, electrons are the majority carrier and are transported through a conduction band (CB) composed of delocalized s orbitals of metal ions, whereas in corresponding p-type materials, the valence band maximum (VBM) for transport of the majority hole carriers is composed of localized p orbitals of oxygen ions. Due to these characteristics of MOSs, electrons injected into MOS thin films are easily transferred along the conducting path and show better mobility regardless of structure ordering, relative to holes. Nevertheless, researchers have persistently studied p-type MOSs because they are necessary to fabricate inverters and/or logic circuits for low power consumption, application to transparent devices, etc.[3]

Stannous oxide (SnO) as a p-type MOS has a relatively large optical band gap of 2.7 eV, and thus has high visible transmittance of above 80 %.[4, 5] Recently, it has been reported that in a SnO film the delocalized 5s orbitals of Sn^{2+} at the edge of the VB could be controlled to have energy levels similar to that of the O 2p orbitals, thereby yielding high hole mobility in the resulting

RSC Advances Accepted Manuscript

TFTs.[6] It is known that Sn has the dual valency of 2+ and 4+. N-type SnO_2 (Sn^{4+}) has a rutile structure with a tetragonal unit cell; in this structure, the Sn and O atoms have coordination numbers of 6 and 3, respectively. In contrast, p-type SnO (Sn^{2+}) has a layered litharge structure having a $Sn_{1/2}$–O–$Sn_{1/2}$ sequence in the [001] direction, and wherein each Sn and O atom form a tetragonal unit.[7, 8]

Due to competition arising from the dual valency of Sn, Sn-based oxide films sputtered under an oxygen partial pressure (P_O) contain three phases: metallic Sn, SnO, and SnO_2. In accordance with this, it has been recently reported that the different oxidized states of Sn in the corresponding thin films yield discernible differences in electrical, optical and micro structural properties of SnO_x films prepared by magnetron sputtering.[4, 9-12] In particular, in the previous researches on the p-type SnO_x based devices, the morphological evolution and related electrical properties in the SnO_x thin films have been overlooked even though the morphological property can influence substantially the resulting electrical properties in other transparent oxide semiconductor TFTs.[13, 14] Only a couple of studies have mentioned on the microstructural evolutions by the heat treatment conditions where the clear explanations for the differences in the electrical properties in the SnO_x thin films and resulting TFTs were not explicitly discussed.[15, 16] Accordingly, to achieve high performance in the p-type SnO_x based field-effect transistors, systematic studies are still required to reveal out the oxidation state and/or microstructure dependency of their electrical properties.

In the present work we investigated the microstructural, morphological evolutions, phase transitions, and related electrical properties of SnO_x thin films and their TFTs sputtered under conditions of various P_O, before and after heat treatment at various temperatures (T_A). The SnO_x film prepared at the lowest P_O of 4 % and subsequently heat-treated at 210 °C consisted of

RSC Advances Accepted Manuscript

dendritic phases and irregular protrusions of metallic Sn, which were facilitated by the oxygen-deficient stoichiometry in the films. These imperfect phases in the SnO_x thin films could be eliminated by increasing P_O conditions up to 8 % during fabrication. The resulting p-channel SnO_x TFTs which were fabricated under P_O of 4 % and subsequently heat-treated at 210 ^oC showed poor field effect mobility (μ_{FE}) of 0.73 cm^2 V^{-1} s^{-1} and low on and off current ratio ($I_{ON/OFF}$) less than 10. Whereas the resulting TFTs prepared at the higher P_O of 8 % showed much improved mobilities up to 2.8 cm^2 V^{-1} s^{-1} and $I_{ON/OFF}$ of above 10^3, which underscores the critical role of the homogeneous ordered aggregates without dendritic phases and irregular protrusions of metallic Sn hindering hole carrier conduction and acting as bulk trap states in this material. By increasing T_A from 210 to 300 °C, the μ_{FE} and $I_{ON/OFF}$ of p-channel SnO_x TFTs fabricated at P_O under 8 % were much degraded, which was attributed by the disproportionation reaction of SnO_x thin films ($2SnO \rightarrow SnO_2 + Sn$).

2. Experimental Methods

2.1 Materials and Device Preparation: A 100-nm-thick SiO_2 layer thermally grown on a highly doped Si wafer was used as a gate dielectric. SnO_x thin films were deposited on a SiO_2/Si substrate at room temperature by means of reactive DC magnetron sputtering with a Sn target (99.999 %, 3 inch diameter), under a processing pressure of about 5×10^{-3} Torr (0.67 Pa); the target-to-substrate distance was approximately 15 cm and the plasma power of 50 W was applied. Various oxygen partial pressures ($P_O = O_2$ / ($Ar + O_2$), vol.%) from 4 to 12 % were applied to prepare various film samples. As-deposited SnO_x thin films were then heat-treated for 1 h inside an Ar-purged tube furnace (above 5 Torr) in order to minimize external oxygen

RSC Advances Accepted Manuscript

participation in film formation; various heat treatment temperatures (T_A) from 150 to 300 °C were applied. For the SnO TFTs, 70-nm-thick Pt electrodes as top contact source/drain (*S/D*) electrodes were deposited on the $SnO_x/SiO_2/Si$ substrate by means of e-gun evaporation. The isolated SnO channel and S/D electrodes were patterned through a shadow mask during each layer deposition. The channel width (*W*) and length (*L*) of the fabricated SnO TFTs were 300 μm and 1000 μm, respectively.

2.2 Characterization: The thickness of each SnO_x thin film sample was measured by means of spectroscopic ellipsometry (SE, ESM-300, J.A. Woollam). Each sample's chemical composition was analyzed by means of X-ray photoelectron spectroscopy (XPS, VG Thermo Scientific, Sigma Probe) under illumination by a monochromatic Al K_α source (≥15 keV). Synchrotron-based grazing-incidence X-ray diffraction (GIXD) analysis of sample films on their SiO_2/Si substrates was conducted at the 9A and 6D beamlines of the Pohang Accelerator Laboratory in Korea. Crystalline phases in these SnO_x films were characterized by using transmission electron microscopy (TEM, Tecnai F20, FEI). Additionally, film morphologies were observed by means of scanning electron microscopy (SEM, Sigma, Carl Zeiss) and atomic force microscopy (AFM, Multimode 8, Bruker).

Resistivity and carrier concentration of the SnO_x thin films were evaluated using a four-point probe (CMT-SR1000N, Advanced Instrument Technology), and van der Pauw measurements of Hall mobility were conducted using a Hall effect measurement system (HL 5500PC, Bio-Rad).[17] Electrical characteristics of the SnO_x TFTs were measured in a room-temperature dark chamber, using a semiconductor parameter analyzer (HP4155A, Hewlett-Packard).

3. Results and Discussion

RSC Advances Accepted Manuscript

3.1. Chemical composition variations among the SnO_x thin films

The chemical compositions of the SnO_x films fabricated at various P_O conditions were evaluated based on deconvoluted XPS spectra. To minimize the contributions of native oxide layers on the topmost layers of the SnO_x films, each sample was subjected to Ar sputtering (2 kV, 3 mA) for 2 s prior to XPS analysis. **Figure 1** shows Sn $3d_{5/2}$ and O 1s XPS core-level spectra of 15-nm-thick SnO_x films fabricated under various P_O from 4 to 12 %, before and after heat treatment. Here, the heat treatment was performed at 210 ^oC for 1h, which resulted in the best electrical properties. Note that all binding energies were calibrated by setting the C 1s peak position at 284.8 eV. Hereafter, SnO_x film samples fabricated under the P_O condition of 4 % are referred to as "4 % P_O samples", and so forth.

The binding energy states of the Sn $3d_{5/2}$ core level yielded XPS peaks around 484.4, 485.9, and 486.6 eV, originating from oxidized states of Sn with three different oxidation numbers (i.e., Sn^0, Sn^{2+}, and Sn^{4+}, respectively).[18, 19] XPS analysis of the Sn $3d_{5/2}$ core level in the SnO_x sample prepared at the lowest P_O of 4 % indicated large portions of Sn^0 and Sn^{2+}: 52.2 and 45.0 at.%, respectively. With increasing P_O, the as-deposited films contained lesser portions of metallic Sn (Sn^0), and no Sn^0 was observed for the 12 % P_O sample: in this case, the Sn^{4+} state was also observed (see red curves around 486.6 eV in **Figure 1**). After the films were heat-treated at 210 °C for 1 h, most of the Sn^0 in the films was found to have oxidized to form SnO. Additionally, XPS spectra of the O 1s core levels in these SnO_x films showed discernible oxygen states, depending on P_O and heat treatment conditions. The binding energies of O–Sn^{2+} and O–Sn^{4+} were assigned as 529.8 and 530.4 eV, respectively.[4, 18-22]

RSC Advances Accepted Manuscript

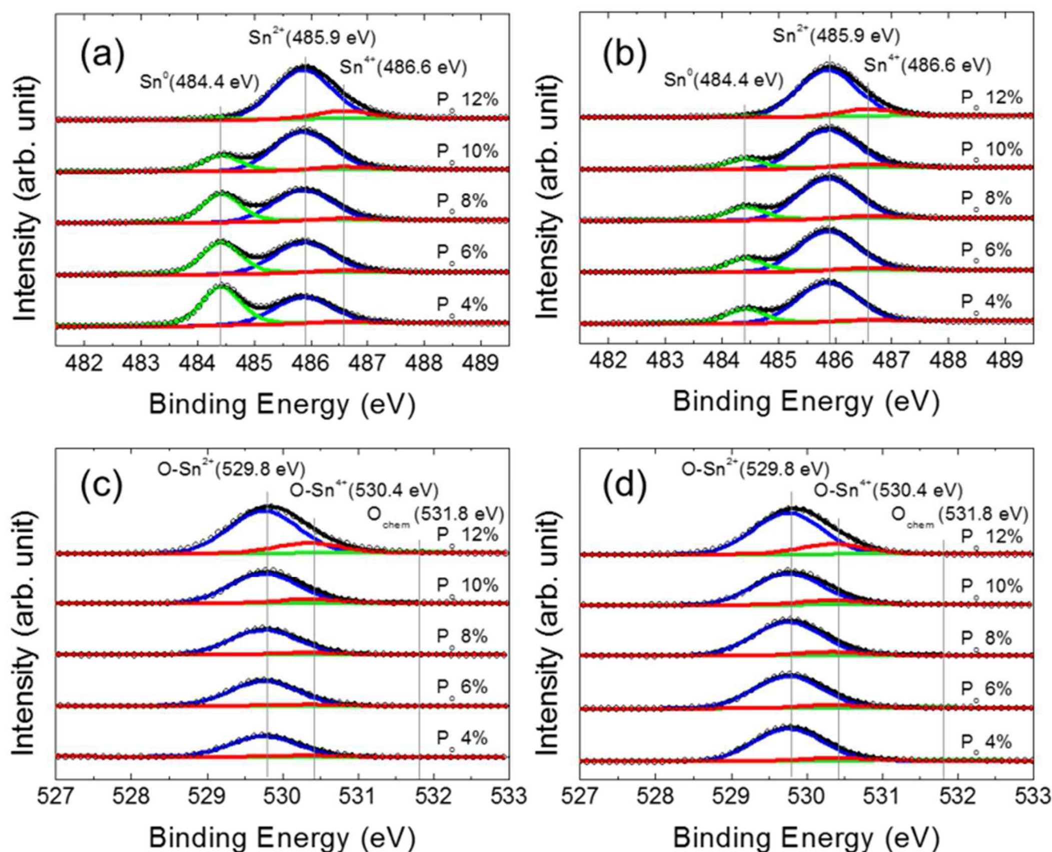

Figure 1. XPS spectra of (a, b) Sn $3d_{5/2}$ and (c, d) O 1s core levels in 15-nm-thick SnO_x thin films deposited on SiO_2 dielectrics under various P_O conditions (4 to 12 %), (a, c) before and (b, d) after heat treatment at 210 °C for 1 h: open black circles represent the measured spectra; blue, red, and green lines respectively represent the deconvoluted Sn^{2+} (or O-Sn^{2+}), Sn^{4+} (or O-Sn^{4+}), and Sn^0 (or O_{chem}, chemisorbed oxygen) spectra, and the black line represents the sum of these deconvoluted spectra.

Figure 2 is based on the XPS results and represents variations in the oxygen content and Sn oxidization states (Sn^0, Sn^{2+}, Sn^{4+}) among SnO_x films fabricated under various P_O conditions, before and after heat treatment at 210 °C for 1 h. The detailed compositional variations were summarized at Table S1 in the SI. The oxygen content in as-deposited SnO_x thin films increased

RSC Advances Accepted Manuscript

monotonically from 24.3 to 43.5 at.% with increasing P_O from 4 to 12 %. As P_O was increased, the resulting portions of Sn^0 decreased from 52.2 to 3.3 % and the portions of Sn^{2+} and Sn^{4+} respectively increased from 45.0 to 84.7 at.% and from 2.8 to 12.1 at.%. During heat treatment, the metallic Sn atoms in the as-deposited films seemed to be mostly oxidized to Sn^{2+} instead of to Sn^{4+} (**Figure 2b**): the portions of Sn^{4+} in the SnO_x films were almost the same before and after heat treatment.

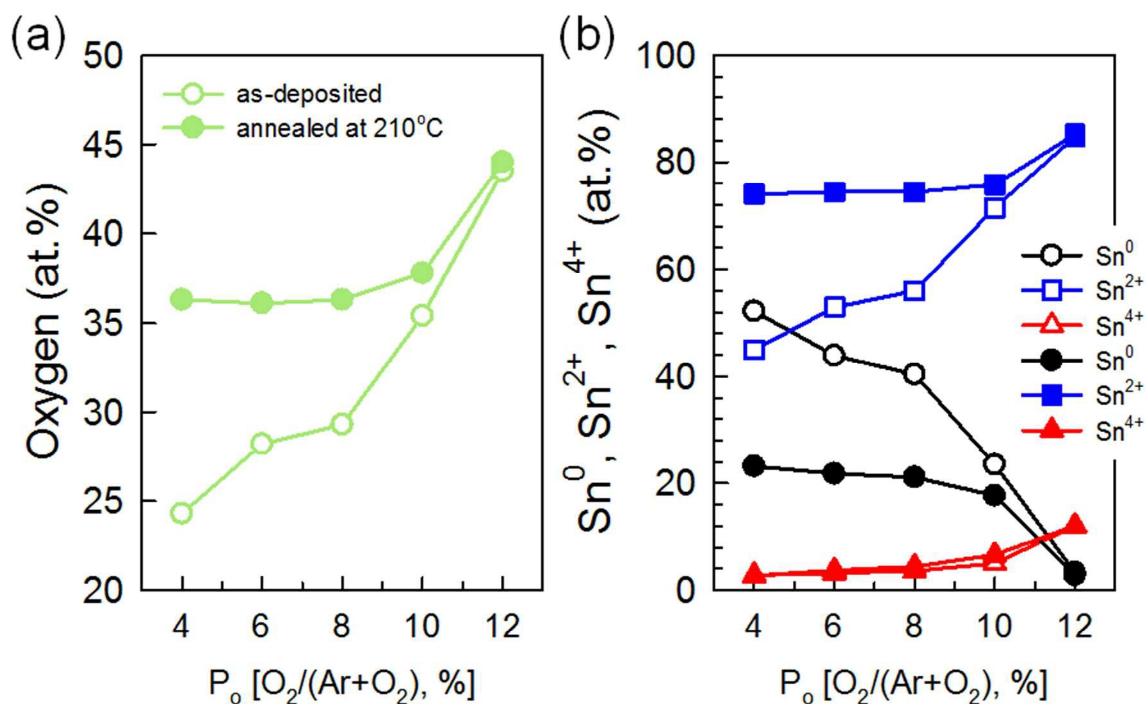

Figure 2. Chemical compositions of SnO_x films fabricated under various P_O conditions before and after heat treatment at 210 °C for 1 h: (a) O, (b) Sn^0, Sn^{2+}, and Sn^{4+}. Open and closed marks respectively represent compositions before and after heat treatment at 210 °C for 1 h.

3.2. Structural and morphological characteristics

Film structure was characterized by means of synchrotron-based GIXD and TEM analyses. First, 15-nm-thick SnO_x films were subjected to two-dimensional (2D) GIXD, which revealed

RSC Advances Accepted Manuscript

Sn, SnO, and SnO_2 phases of different portions, depending on their P_O and heat treatment conditions. Among the as-deposited SnO_x films on SiO_2/Si substrates, the 4 and 6 % P_O samples showed weak X-ray reflections at Q of 2.155, 2.250, and 3.048 $Å^{-1}$ (**Figures S1a** and **b** in the SI), originating from (200), (101), and (220) crystal planes in β phases of Sn (JCPDS No. 01-086-2264),[23-25] whereas films fabricated under higher P_O showed only a hollow ring at Q = 2.064 $Å^{-1}$ in the 2D GIXD patterns (**Figures S1c** and **d** in the SI), indicating amorphous structure.

After heat treatment at 210 °C for 1 h, except for the 10% P_O sample, all SnO_x films showed intense X-ray reflections in 2D GIXD patterns that indicated ordered phases of metallic or oxidized Sn (**Figure 3**). For the 4, 6, and 8 % P_O samples, intense X-ray reflections were observed that corresponded to polycrystalline SnO (JCPDS No. 01-085-0712) as well as β-phase Sn residue (see arrow-marked peaks in **Figure 3**). For heat-treated 4, 6 and 8 % P_O samples, typical X-ray reflections were observed at Q of 1.297, 2.101, 2.334, and 2.594 $Å^{-1}$, originating from the (001), (101), (110), and (002) planes in SnO crystallites with tetragonal unit cells: $a = b$ = 3.796 Å, c = 4.816 Å.[8] The X-ray reflections were anisotropically distributed along the X-ray Debye rings (**Figure 3**), suggesting that the SnO aggregates were preferentially oriented with respect to the substrates. Interestingly, the heat-treated 8 % P_O SnO_x film showed quite discernible orientations of (101), (110), and (200) planes in comparison to those in the 4 and 6 % P_O samples (this will be discussed later). However, the SnO_x film samples with the highest O content (the 10 and 12 % P_O samples) retained amorphous-like structures even after heat treatment, suggesting that the presence of the secondary SnO_2 phase strongly prevented crystallization and ordering of the primary SnO phase (approximately 76 at.%, determined by XPS analysis). The XPS and GIXD results strongly supported the conclusion that the order of

RSC Advances Accepted Manuscript

structures in the as-deposited and heat-treated SnO_x films was degraded severely with increasing SnO_2 composition.[4]

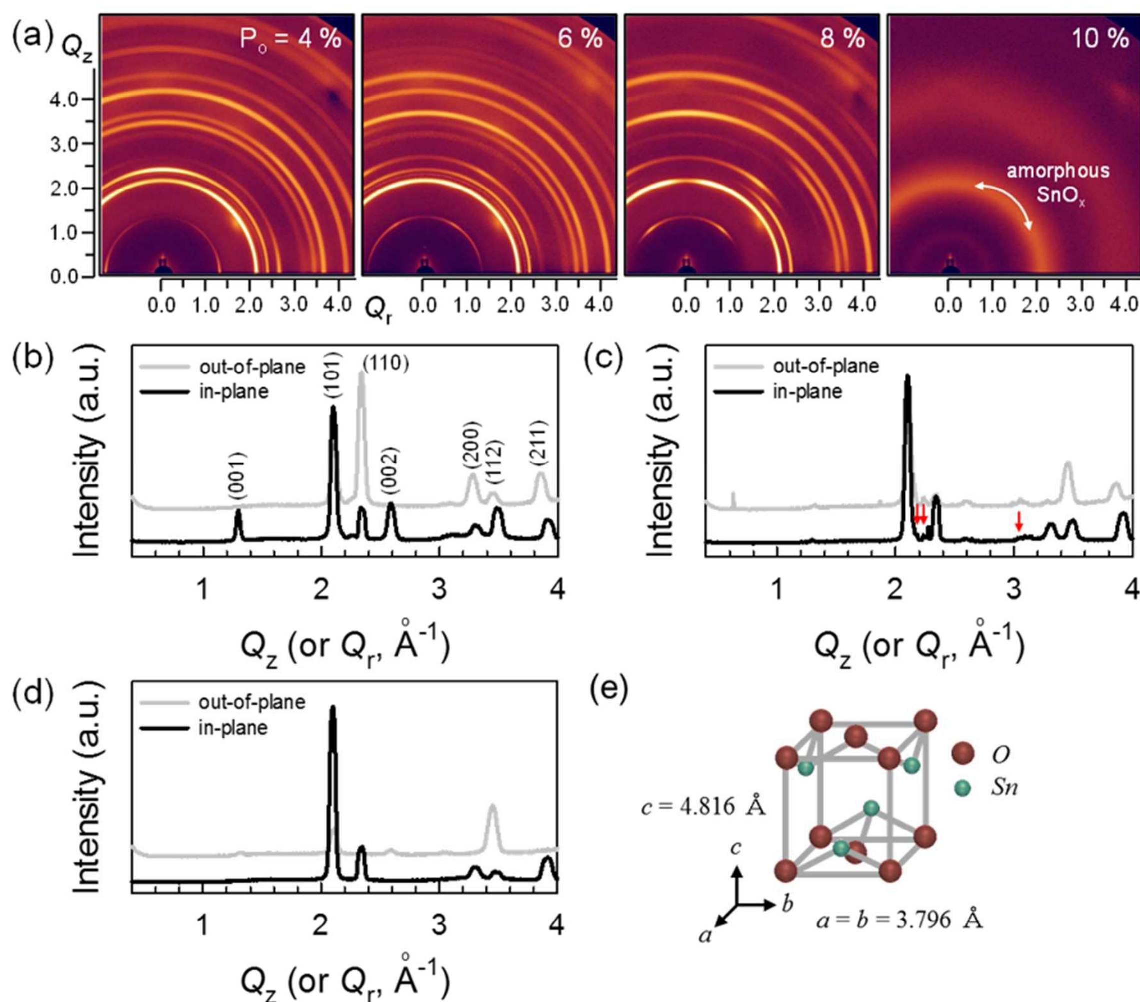

Figure 3. (a) 2D GIXD patterns of SnO_x films fabricated under P_O of 4, 6, 8, and 10 % and heat-treated at 210 °C for 1 h. (b–e) 1D in-plane and out-of-plane X-ray profiles extracted from the patterns shown in (a): (b) 4, (c) 6, and (d) 8 % P_O samples; (e) unit cell of the SnO lattice.[3, 7] Weak X-ray reflections marked with red arrows marked in (c) correspond to the β phase of Sn.

Figure 4 shows in-plane TEM micrographs of 15-nm-thick SnO_x films fabricated under the P_O of 4 and 8 % and then heat-treated at 210 °C for 1 h. The 4 % P_O sample consisted mostly of

RSC Advances Accepted Manuscript

polycrystalline SnO in which the (001) and (101) crystal planes were oriented normal to the dielectric surface (**Figure 4a** inset). Additionally, less ordered grain boundaries were observed having 5–10 nm gaps (see broken line–marked region in **Figure 4a**). In contrast, the SnO crystallites in the heat-treated 8 % P_O sample did not show any visible grain boundary: the (110) and (101) crystal planes were preferentially oriented normal to the dielectric surface (**Figure 4b**). In this case, the angle between (110) and (101) planes was found to be about 64°, close to calculated value of 64.04° for the previously reported typical tetragonal structure of SnO.[8] It was also found that the [001] direction (c-axis) in these crystallites was tilted from the surface normal, as evidenced by the 2D GIXD pattern (**Figure 3a**). During reactive DC magnetron sputtering with a Sn target, fine control of P_O is important to achieve preferential development of p-type SnO crystallites on dielectric surfaces; this leads to a discernible difference in the electrical properties of the resulting TFTs, as will be discussed below.[26]

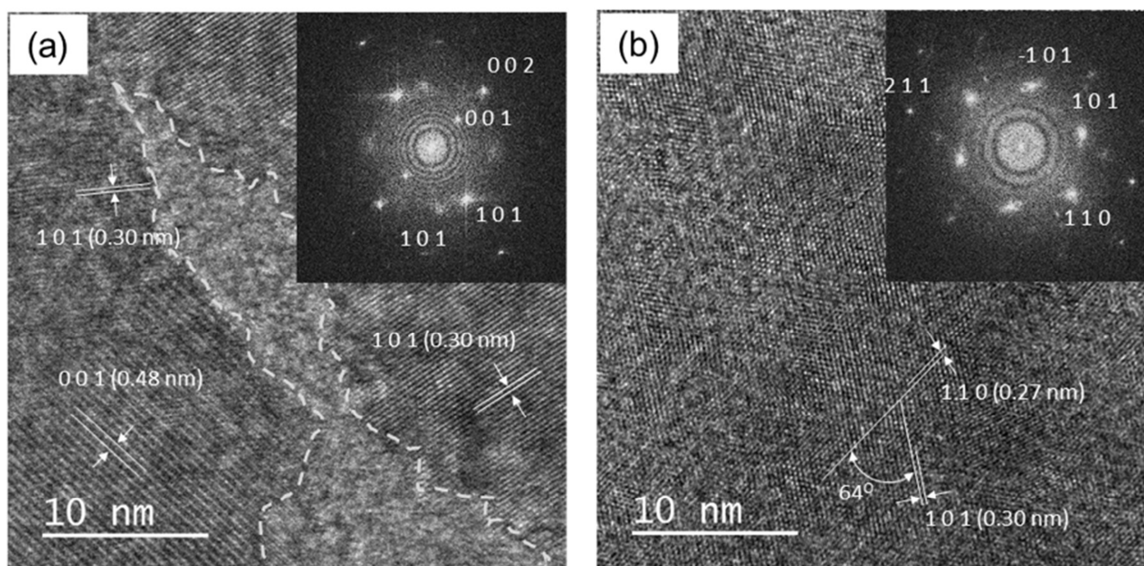

Figure 4. High-resolution TEM micrographs (plan-view) of 15-nm-thick SnO_x films fabricated under P_O of (a) 4 and (b) 8 %, and both subsequently heat-treated at 210 °C for 1 h. Insets depict fast Fourier transform patterns corresponding to the micrographs.

RSC Advances Accepted Manuscript

Additional SEM and AFM analyses were carried out to investigate the morphologies of the SnO_x thin films. All the as-deposited films showed very smooth and featureless morphologies, regardless of the P_O during their fabrication (**Figure S2**). However, the heat-treated films all showed discernible structures that depended on the processing parameters of P_O and T_A. An SEM micrograph of the heat-treated 4 % P_O film showed a percolated layer including dendritic phases of widths ranging from 20 to 100 nm and vertically grown irregular protrusions with diameters on the order of several tens of nanometers. The dendritic grains and aggregates caused considerable inhomogeneity in this SnO_x film, specifically, yielding severe lateral disconnection (**Figure 5a and Figure S5 in SI**). The irregular protrusions were determined by means of energy dispersive X-ray spectroscopy (EDS) analysis to be metallic Sn aggregates (**Figure S3**). The crystallites and aggregates in the 210 °C-heat-treated SnO_x films became denser and less numerous with increasing P_O (Figure 5b, c). In contrast, the 10 % P_O samples showed featureless and smooth morphologies both before and after heat treatment (Figure 5d).

RSC Advances Accepted Manuscript

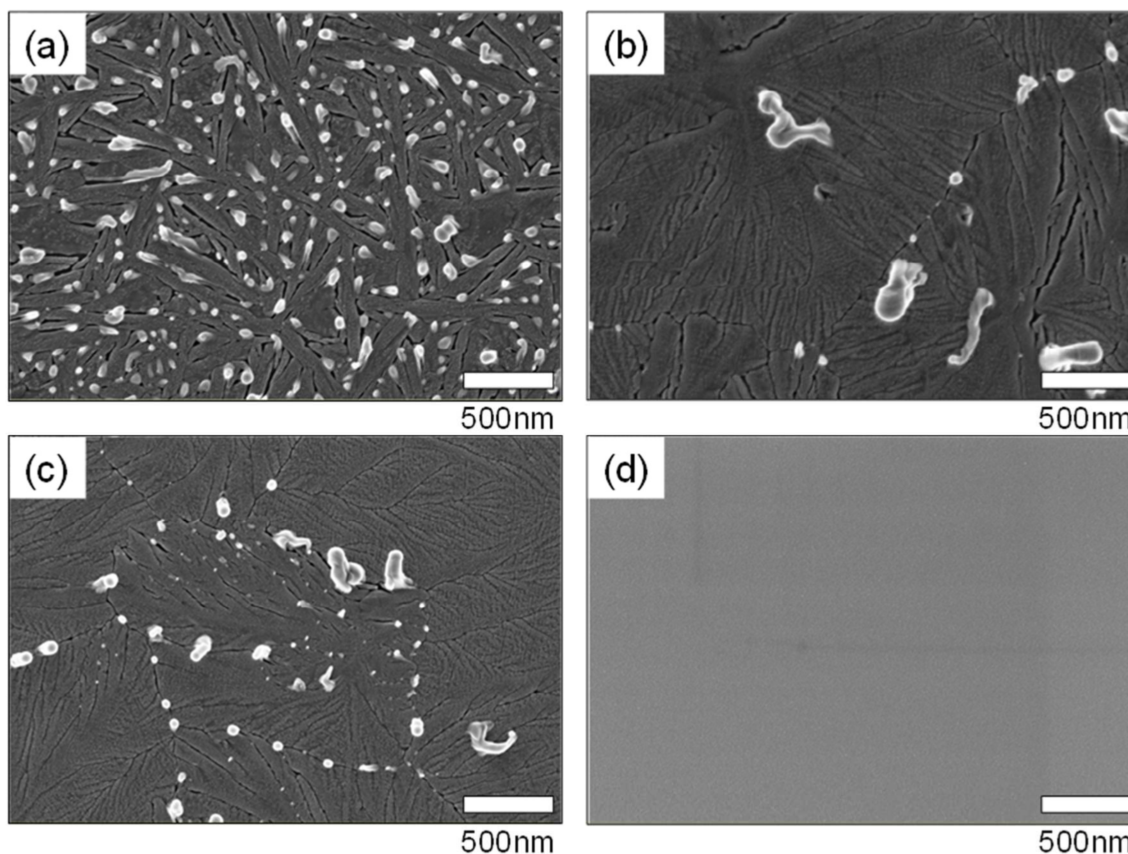

Figure 5. SEM micrographs of SnO_x thin films fabricated under various P_O and subsequently heat-treated at 210 °C for 1 h: (a) 4, (b) 6, (c) 8, and (d) 10 % P_O samples.

Additionally, AFM topography analyses of the corresponding SnO_x films showed similar morphologies as those indicated by the SEM results: increased oxygen content in the heat-treated SnO_x films reduced the phase inhomogeneity and film surface roughness (R_q) (**Figure 6**). R_q of the heat-treated films decreased drastically from 20.5 nm (at P_O = 4 %) to 0.4 nm (at P_O = 10 %) with increasing P_O during their fabrication. Particularly, the R_q of 10 % P_O SnO_x film was not changed after heat treatment at T_A of 210 °C. The SEM and AFM results strongly supported the conclusion that the SnO_x phase formation was very sensitive to oxygen stoichiometry and an equivalent oxygen stoichiometry was required to form the homogeneous p-type SnO phase from the as-deposited films.

RSC Advances Accepted Manuscript

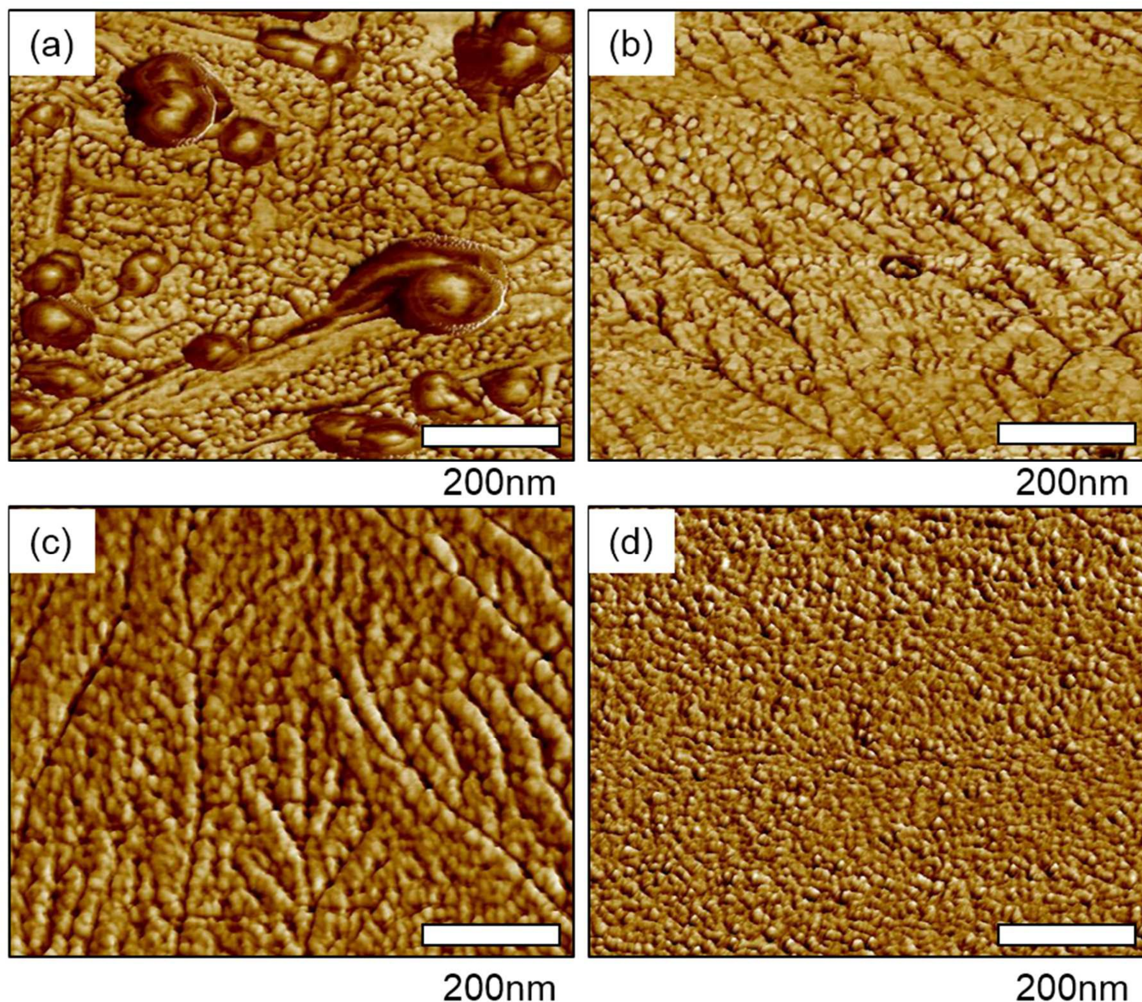

Figure 6. AFM phase images of SnO_x films fabricated under various P_O and subsequently heat-treated at 210 °C: (a) 4, (b) 6, (c) 8, and (d) 10 % samples.

Several studies have shown that the evolution of dendritic structures is enhanced when crystal growth rate exceeds the mass transport rate of ions and molecules that are necessary for crystal growth.[27, 28] Especially, Boggs et al.[29] suggested reasonable mechanisms for the dendritic crystal growth of polycrystalline SnO phases during crystallization of SnO_x thin films under oxygen-deficient conditions. Namely, they suggested that the areas adjacent to the crystallized SnO lattices become depleted in oxygen as the oxygen is captured and integrated into SnO lattices;

RSC Advances Accepted Manuscript

consequently, further growth of SnO crystals must be directed toward areas that are richer in oxygen.

As shown in **Figure 2a**, the SnO_x thin films in this work were all deposited under oxygen-deficient conditions and then heat-treated in an oxygen-deficient atmosphere. Accordingly, the observation in the present work of the evolution of dendritic structures on surfaces of heat-treated SnO_x thin films can be attributed to dendritic crystal growth of polycrystalline SnO phases in oxygen-deficient environments. Consequently, metallic Sn compositions in the oxygen-deficient areas adjacent to the dendritic structures would steadily increase until they exceeded their solubility limit, leading to phase separation and the formation of metallic Sn irregular protrusions. This explanation is supported well by the gradual disappearance of dendritic structures and irregular protrusions of metallic Sn observed with increasing P_O from 4 to 8 %. The reason why the heat-treated 10 % P_O sample showed a uniform surface is that the film had not yet crystallized.

3.3. Electrical properties and functionalities

The electrical resistivity (ρ), net free carrier concentration, and Hall mobility (μ_{Hall}) of the SnO_x thin films were evaluated. **Figure 7a** shows the ρ values of 15-nm-thick SnO_x thin films prepared under various P_O (4–12 %) and T_A (165–300 °C) conditions. The as-deposited 4 % P_O film had ρ of 10^{-1} Ω cm, suggesting its feasibility for use as a semiconductor. Increasing the P_O used during film preparation increased the resistivity of the resulting SnO_x films. Thus, the as-deposited 10 % P_O sample showed the increased ρ value of 10^2 Ω cm. In contrast, the 12 % P_O sample exhibited insulator-like properties whereby it was difficult to measure ρ because of the high contact resistance. The films' ρ values could be tailored by controlling T_A. Heat treatment at

RSC Advances Accepted Manuscript

T_A = 165 °C caused the resistivities to increase by 1 to 3 orders of magnitude relative to those of the as-deposited films. When the as-deposited films were heat-treated at T_A of 210 °C or greater, the SnO_x films fabricated under P_O ranging from 4 to 8 % exhibited T_A-independent ρ values ranging from 10^0 to 10^1 Ω cm. On the other hand, those films fabricated under P_O of 10 and 12 % showed insulator-like behaviors. Considering the previously discussed evolution of chemical states and crystal structures, the observation of increased ρ with increasing P_O for the as-deposited films is well consistent with the fact that the portion of metallic Sn decreased with increasing P_O. Oxidative deposition would decrease the metal Sn fraction, leading to enhanced electrical resistance. On the other hand, the strong T_A dependency of ρ observed for the SnO_x films deposited with P_O of 4 to 8 % seems to have been associated with the microstructural transition from amorphous SnO_x to polycrystalline SnO. Note that the amorphous phase of the insulator-like 10 and 12 % P_O films was maintained after heat treatment at various T_A.

Heat-treated semiconducting SnO_x films (T_A = 210 °C) were subjected to Hall effect measurements, in which they exhibited relatively high thermal stability. **Figure 7b** shows net carrier concentration and μ_{Hall} values for the SnO_x thin films versus the P_O used during their fabrication. The dominant carrier conduction for the 4, 6, and 8% P_O films was determined to be p-type. The net hole concentration (N_h) for the SnO_x films monotonically decreased from 4.35×10^{18} to 1.81×10^{18} cm^{-3} with increasing P_O. This can be attributed to a reduction in free hole carriers in the overall SnO_x film as the n-type SnO_2 phase present in the film increases with increasing P_O (see **Table S1 in the SI**).[4] Conversely, the films' μ_{Hall} values increased from 1.1 to 5.5 cm^2 V^{-1} s^{-1} with increasing P_O. The differences in crystallographic preferential orientation and topological evolution of the SnO_x film depending on P_O during deposition can be considered the most plausible origin for the observed variation in μ_{Hall}. The electronic structure reported by

RSC Advances Accepted Manuscript

Togo el al.[6] suggests that the stannous oxide (SnO) has an anisotropic band structure in its Brillouin zone. The curvature of the *E-k* diagram in the [001] direction (Γ-Z) is larger than those in the [100] direction (Γ-X) and [110] direction (Γ-M) near the VBM. This means that the effective hole mass (m^*_h) in the [001] direction is the smallest among the various directions. From this, one would predict that 4 % P_O films showed higher mobility than 8 % P_O films because the volume faction of [001] oriented parallel to the in-plane direction was substantially higher in the former, however, as shown in **Figure 7b**, this is not the case. In general, the carrier mobility is proportional to the product of the mean scattering time and inversely proportional to the effective mass. Therefore, it can be inferred that the carrier scattering mechanism plays a critical role in determining the carrier mobility. Indeed, the 4 % P_O film suffered from microstructural inhomogeneities such as metallic Sn aggregates and dendritic structure. These imperfections are likely to act as strong scattering centers, and thus to be responsible for this material's inferior mobility.

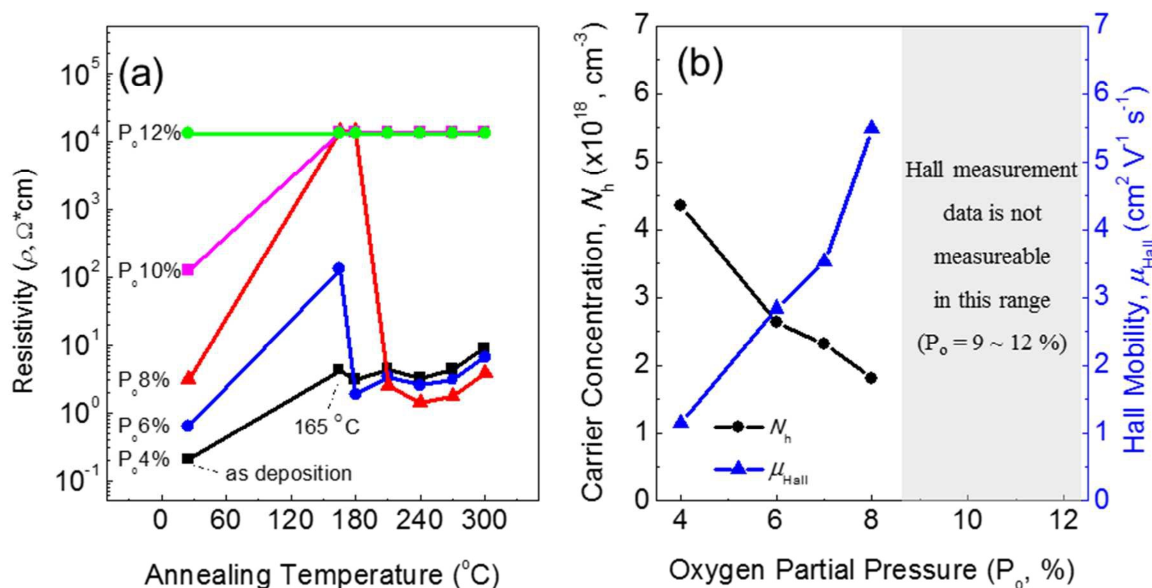

RSC Advances Accepted Manuscript

Figure 7. (a) Resistivity of SnO_x thin films (15-nm-thick) deposited under various P_O (4 to 12 %) before and after heat treatment (165–300 °C). (b) Net hole concentration (N_h) and Hall mobility (μ_{Hall}) of SnO_x thin films heat-treated at 210 °C, as acquired during Hall effect measurements.

The electrical functionality of these p-type semiconducting SnO_x films was further evaluated in thin-film transistors (TFTs) made from the films. **Figure 8a** shows representative transfer characteristics for bottom gate SnO_x TFTs with 15-nm-thick channels made using the 4, 6, and 8 % P_O films. The field-effect mobility (μ_{FE}) and subthreshold gate swing (SS) were respectively calculated using equations [1] and [2], given below. The maximum bulk trap density ($N_{SS,max}$) and interfacial trap density ($D_{it,max}$) were evaluated using equation [3], for which the value of $N_{SS,max}$ ($D_{it,max}$) was estimated by setting the $D_{it,max}$ ($N_{SS,max}$) term to zero.

$$\mu_{\mathrm{FE}} = \frac{L \times g_{\mathrm{m}}}{W \times C_{\mathrm{i}} \times V_{\mathrm{DS}}}, \text{where } g_{\mathrm{m}} = \frac{\partial I_{\mathrm{DS}}}{\partial V_{\mathrm{GS}}}\Big|_{V_{\mathrm{DS}} = \text{constant}} \quad [1]$$

$$SS = \left(\frac{\partial \log(I_{\mathrm{DS}})}{\partial V_{\mathrm{GS}}}\right)^{-1}\Big|_{\max} \quad [2]$$

$$SS = q k_{\mathrm{B}} T (N_{\mathrm{SS,max}} t_{\mathrm{ch}} + D_{\mathrm{it,max}})/[C_{\mathrm{i}} \log(e)] \quad [3]$$

Here, L is the channel length (300 μm), W is the channel width (1000 μm), C_i is the capacitance per unit area of the gate dielectric (34.5 nF cm^{-2}), V_{DS} is the drain voltage, I_{DS} is the drain current, V_{GS} is the gate bias, q is the electron charge, k_B is the Boltzmann constant, T is the absolute temperature, and t_{ch} is the channel layer thickness (15 nm).[30]

RSC Advances Accepted Manuscript

All the SnO_x TFTs exhibited p-type conduction irrespective of the P_O values. The SnO_x TFT prepared at P_O = 4 % showed the marginal μ_{FE} of 0.73 $cm^2\ V^{-1}\ s^{-1}$, and yielded the low $I_{ON/OFF}$ ratio of 6.8, representing poor current modulation capability. The device performance of the SnO_x TFTs was improved for films deposited under greater P_O. The high μ_{FE} of 2.8 $cm^2\ V^{-1}\ s^{-1}$ and reasonable $I_{ON/OFF}$ ratio of 1.0×10^3 were achieved by the SnO_x TFT based on the 8 % P_O film, as shown in **Figure 8a** and **Table 1.** The superior performance of the SnO_x TFT based on the 8 % P_O film underscores the importance of its homogenous ordered aggregate state and its absence of Sn metal aggregate and abrupt dendritic structure.

It is interesting to discuss why the SnO_x TFT based on the 4 % P_O film yielded the poor $I_{ON/OFF}$ ratio of 6.8. The observation of high off-state I_{DS} indicated the difficulty in fully depleting the bulk semiconducting SnO_x film. In other words, the quasi Fermi level (E_F) in the SnO_x film near the gate dielectric/semiconductor interface was strongly pinned due to the very large N_{SS} because E_F cannot move upward without trap filling.[31] Indeed, the extracted $N_{SS,max}$ value for the TFTs based on 4 % P_O film was the largest measured (1.5×10^{20} $eV^{-1}\ cm^{-3}$). Contrastingly, $N_{SS,max}$ for the TFTs based on 8 % P_O film was 2.0×10^{19} $eV^{-1}\ cm^{-3}$. The superior transporting property of these TFTs was clearly reflected in the higher I_{DS} level of their output characteristics (see **Figure 7b**).

A qualitatively similar trend for the p-channel SnO_x TFTs based on the 4, 6, and 8 % P_O films heat-treated at T_A of 210 °C was also observed for higher T_A (240, 270, and 300 °C; **Figure S4**). Interestingly, the μ_{FE} value and $I_{ON/OFF}$ ratio observed for a SnO_x TFT at a given P_O condition were degraded by increasing T_A from 210 to 300 °C. For example, the TFTs based on the 8 % P_O film and heat-treated at 300 °C yielded μ_{FE} of 1.0 $cm^2\ V^{-1}\ s^{-1}$ and the $I_{ON/OFF}$ ratio of 1.6×10^2. This behavior can also be attributed to a structural transition involving the chemical states of Sn

RSC Advances Accepted Manuscript

ions and microstructural inhomogeneity, namely, phase separation from 2SnO to SnO_2 plus metallic Sn; this transition is thermodynamically driven above 250 °C.[32, 33]

Finally it would be meaningful to compare the performance of SnO TFTs in this study with other works. The μ_{FE} of 2.8 $cm^2\ V^{-1}\ s^{-1}$ and $I_{ON/OFF}$ ratio of 1.0×10^3 for the SnO_x TFT based on the 8 % P_O film are comparable to those (μ_{FE} : 1.7 ~ 6.8 $cm^2\ V^{-1}\ s^{-1}$, $I_{ON/OFF}$ ratios of $10^3 \sim 10^4$) reported in the literature for other p-channel oxide TFTs.[4, 11, 15, 34-38] It should be noted that higher mobility ($\geq$ 3.3 $cm^2\ V^{-1}\ s^{-1}$) can be achieved further by adopting the high permittivity dielectric films such as HfO_2,[11] $AlTiO_x$,[36] and/or reducing the gate insulator thickness.[34, 35]

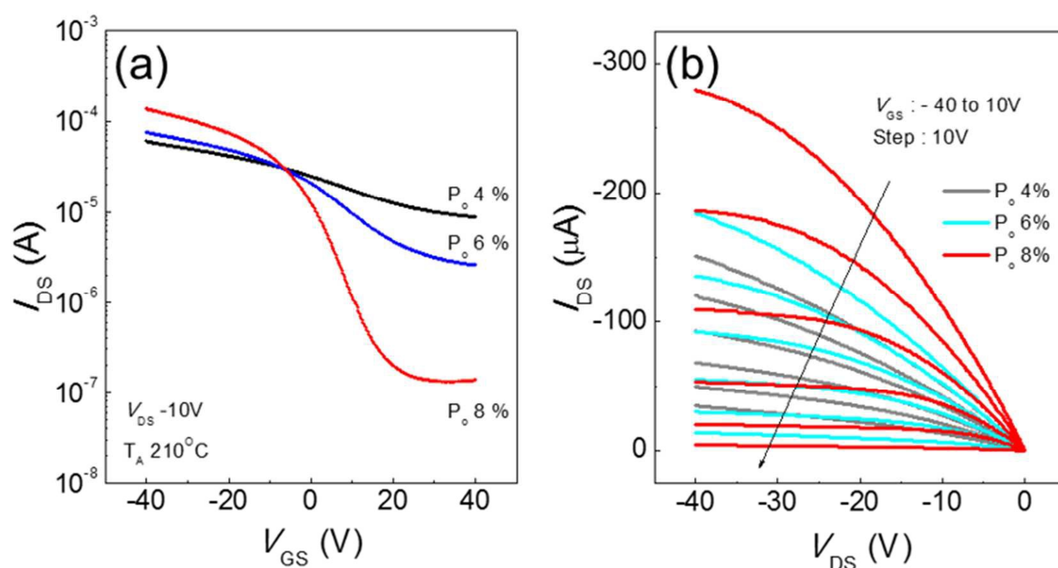

Figure 8. (a) Transfer and (b) output characteristics of bottom gate structure TFTs based on thin SnO_x films (15-nm-thick) fabricated under various P_O (4, 6, and 8 %) and heat-treated at 210 °C.

Table 1. Summary of electrical characteristics of the SnO_x thin films and TFTs: net carrier concentration (N_h), Hall mobility (μ_{Hall}), $I_{ON/OFF}$ ratio, field effect mobility (μ_{FE}), subthreshold

RSC Advances Accepted Manuscript

swing (*SS*), maximum bulk trap density ($N_{SS,max}$), and interface trap density ($D_{it,max}$). The SnO_x thin films and TFTs were fabricated at various oxygen partial pressures (P_O) from 4 to 12 % and were heat-treated at 210 °C.

P_O (%)	N_h (cm^{-3})	μ_{Hall} ($cm^2 V^{-1} s^{-1}$)	$I_{ON/OFF}$	μ_{FE} ($cm^2 V^{-1} s^{-1}$)	*SS* (V/dec.)	$N_{SS,max}$ ($eV^{-1} cm^{-3}$)	$D_{it,max}$ ($eV^{-1} cm^{-2}$)
4	4.35×10^{18}	1.14	6.8×10^0	0.73	62.9	1.52×10^{20}	2.28×10^{14}
6	2.64×10^{18}	2.84	2.9×10^1	1.21	27.6	6.64×10^{19}	9.96×10^{13}
8	1.81×10^{18}	5.49	1.0×10^3	2.80	8.47	2.03×10^{19}	3.05×10^{13}

Note: The electrical properties of SnO_x thin films fabricated under P_O of 10 and 12 %, and TFTs fabricated based on these films, were not measurable due to their excessive resistivity.

4. Conclusions

The chemical, structural, and electrical properties of SnO_x thin films deposited by means of reactive DC sputtering were tailored by controlling the oxygen partial pressure used during sputtering (P_O = 4–12 %) and the post heat treatment temperature (T_A = 150–300 °C). The as-deposited SnO_x thin films were found to be oxygen-deficient irrespective of the P_O during deposition whereas the chemical state of Sn ions in the heat-treated SnO_x films strongly depended on P_O. Higher P_O conditions, within the range between 4 and 8 %, favored the formation of SnO/SnO_2 phases and the suppression of metallic Sn phase in the resulting heat-treated films. Simultaneously, the preferential orientation of SnO_x films changed from the (001), (101) face to the (101), (110) face with increasing P_O. The SnO_x film fabricated under the lowest P_O studied of 4% consisted of dendritic phases and irregular protrusions of metallic Sn, which are enhanced by the oxygen-deficient stoichiometry. This structural inhomogeneity was weakened with increasing P_O and finally disappeared in the 10 % P_O sample. The P_O- and T_A-

RSC Advances Accepted Manuscript

dependent chemical and structural properties of the SnO_x films were reflected in the electrical performance of the resulting TFTs. TFTs based on a SnO_x channel prepared at P_O of 4 % and T_A of 210 °C exhibited the marginal μ_{FE} of 0.73 $cm^2 V^{-1} s^{-1}$ and the low $I_{ON/OFF}$ ratio of 6.8, which can be attributed to structural imperfections of the film, namely its rough dendritic structure and the presence of metallic Sn clusters. Contrastingly, the 8 % P_O film heat-treated at 210 °C showed a homogeneous ordered aggregates without any dendritic phase or irregular protrusions of metallic Sn, and p-type TFTs based on this film achieved the high μ_{FE} of 2.8 $cm^2 V^{-1} s^{-1}$ and $I_{ON/OFF}$ ratio of ~10^3, underscoring the critical role of this material's superior structure. The μ_{FE} and $I_{ON/OFF}$ ratio performance metrics of the TFTs based on the 8 % P_O films deteriorated as T_A was increased from 210 to 300 °C, indicating that the disproportionation reaction [2SnO → SnO_2 + Sn] should be avoided to ensure optimal transistor performance. Comprehensive understanding of the P_O and T_A dependency of SnO_x films' chemical, structural, and electrical properties would enable useful design concepts for high performance TFTs based on p-channel SnO_x.

ASSOCIATED CONTENT

Supporting Information

Summarizations of the chemical compositions of Sn (Sn^0, Sn^{2+}, and Sn^{4+}) and O content in SnO_x films fabricated under various P_O conditions, Additional details on the 2D GIXD patterns of as-deposited SnO_x films, SEM images of as-deposited SnO_x thin films, Energy dispersive X-ray spectroscopy (EDS) analysis of atomic composition in the irregular protrusions of SnO_x thin films, TFT performance metrics extracted from transfer characteristics of bottom gate TFTs

RSC Advances Accepted Manuscript

prepared using SnO_x thin films, SEM micrographs of 45-nm-thick SnO_x films annealed at 210 °C for 1 h. This material is available free of charge via the Internet at http://www.rsc.org.

AUTHOR INFORMATION

Corresponding Author

[*]J. K. J. (jkjeong1@hanyang.ac.kr); [#]H. Y. (hcyang@inha.ac.kr); [$]H. J. K. (thinfilm@snu.ac.kr)

Author Contributions

The manuscript was written through contributions of all authors. All authors have given approval to the final version of the manuscript.

ACKNOWLEDGMENT

This study was supported by the Industrial Strategic Technology Development Program Funded by MKE/MEIT (10041808) and the National Research Foundation of Korea (NRF) grant funded the Korean government (NRF-2015R1A2A2A01003848 and NRF-2013R1A1A2063963).

ABBREVIATIONS

DC, direct current; MOSs, metal oxide semiconductors; LCs, liquid crystals; OLEDs, organic light emitting diodes; TFTs, thin-film transistors; CB, conduction band; VBM, valence band maximum; *S/D*, source/drain; SE, spectroscopic ellipsometry; XPS, X-ray photoelectron spectroscopy; GIXD, grazing-incidence X-ray diffraction; TEM, transmission electron microscopy; EDS, energy dispersive x-ray spectroscopy; SEM, scanning electron microscopy; AFM, atomic force microscopy.

RSC Advances Accepted Manuscript

References

(1) Nomura, K.; Ohta, H.; Takagi, A.; Kamiya, T.; Hirano, M.; Hosono, H., Room-Temperature Fabrication of Transparent Flexible Thin-Film Transistors Using Amorphous Oxide Semiconductors. *Nature* **2004,** *432* (7016), 488-492.

(2) Ginley, D.; John, P., Transparent Conductors. In *Handbook of Transparent Conductors*, Ginley, D.; Hosono, H.; Paine, D. C., Eds. Springer Science & Business Media: **2010**; pp 1-25.

(3) Fortunato, E.; Barquinha, P.; Martins, R., Oxide Semiconductor Thin-Film Transistors: A Review of Recent Advances. *Adv. Mater.* **2012,** *24* (22), 2945-2986.

(4) Luo, H.; Liang, L. Y.; Cao, H. T.; Liu, Z. M.; Zhuge, F., Structural, Chemical, Optical, and Electrical Evolution of SnO_X Films Deposited by Reactive Rf Magnetron Sputtering. *ACS Appl. Mater. Interfaces* **2012,** *4* (10), 5673-5677.

(5) Ogo, Y.; Hiramatsu, H.; Nomura, K.; Yanagi, H.; Kamiya, T.; Hirano, M.; Hosono, H., P-Channel Thin-Film Transistor Using P-Type Oxide Semiconductor, Sno. *Appl. Phys. Lett.* **2008,** *93* (3), 2113.

(6) Togo, A.; Oba, F.; Tanaka, I.; Tatsumi, K., First-Principles Calculations of Native Defects in Tin Monoxide. *Phys. Rev. B* **2006,** *74* (19), 195128.

(7) Batzill, M.; Diebold, U., The Surface and Materials Science of Tin Oxide. *Prog. Surf. Sci.* **2005,** *79* (2), 47-154.

(8) Moore Jr, W. J.; Pauling, L., The Crystal Structures of the Tetragonal Monoxides of Lead, Tin, Palladium, and Platinum. *J. Am. Chem. Soc.* **1941,** *63* (5), 1392-1394.

RSC Advances Accepted Manuscript

(9) De, A.; Ray, S., A study of the structural and electronic properties of magnetron sputtered tin oxide films. Journal of Physics D: Applied Physics, **1991**, 24(5), 719-726.

(10) Muranaka, S.; Bando, Y.; Takada, T., Preparation by reactive deposition and some physical properties of amorphous tin oxide films and crystalline SnO_2 films. Thin Solid Films, **1981**, 86(1), 11-19.

(11) Caraveo-Frescas, J. A.; Nayak, P. K.; Al-Jawhari, H. A.; Granato, D. B.; Schwingenschlögl, U.; Alshareef, H. N., Record Mobility in Transparent P-Type Tin Monoxide Films and Devices by Phase Engineering. *ACS nano* **2013,** *7* (6), 5160-5167.

(12) Hsu, P.-C.; Hsu, C.-J.; Chang, C.-H.; Tsai, S.-P.; Chen, W.-C.; Hsieh, H.-H.; Wu, C.-C., Sputtering Deposition of P-Type SnO Films with SnO_2 Target in Hydrogen-Containing Atmosphere. *ACS Appl. Mater. Interfaces* **2014,** *6* (16), 13724-13729.

(13) Raja, J.; Jang, K.; Nguyen, H. H.; Trinh, T. T.; Choi, W.; Yi, J., Enhancement of electrical stability of a-IGZO TFTs by improving the surface morphology and packing density of active channel. Current Applied Physics **2013**, 13 (1), 246-251;

(14) Zhang, H. Z.; Cao, H. T.; Chen, A. H.; Liang, L. Y.; Liu, Z. M.; Wan, Q., Enhancement of electrical performance in In_2O_3 thin-film transistors by improving the densification and surface morphology of channel layers. Solid-State Electronics **2010**, 54 (4), 479-483.

(15) Hsu, P.-C.; Wu, C.-C.; Hiramatsu, H.; Kamiya, T.; Hosono, H., Film Texture, Hole Transport and Field-Effect Mobility in Polycrystalline SnO Thin Films on Glass. *ECS J. Solid State Sci. Technol.* **2014,** *3* (9), Q3040-Q3044.

RSC Advances Accepted Manuscript

(16) Toyama, T.; Seo, Y.; Konishi, T.; Okamoto, H.; Tsutsumi, Y., Physical Properties of P-Type Tin Monoxide Films Deposited at Low Temperature by Radio Frequency Magnetron Sputtering. *Appl. Phys. Express* **2011,** *4* (7), 071101.

(17) van der PAUW, L., A Method of Measuring Specific Resistivity and Hall Effect of Discs of Arbitrary Shape. *Philips Res. Rep.* **1958,** *13*, 1-9.

(18) Her, Y.-C.; Wu, J.-Y.; Lin, Y.-R.; Tsai, S.-Y., Low-Temperature Growth and Blue Luminescence of SnO_2 Nanoblades. *Appl. Phys. Lett.* **2006,** *89* (4), 43115-43115.

(19) Szuber, J.; Czempik, G.; Larciprete, R.; Koziej, D.; Adamowicz, B., XPS Study of the L-CVD Deposited SnO_2 Thin Films Exposed to Oxygen and Hydrogen. *Thin Solid Films* **2001,** *391* (2), 198-203.

(20) Larciprete, R.; Borsella, E.; De Padova, P.; Perfetti, P.; Faglia, G.; Sberveglieri, G., Organotin Films Deposited by Laser-Induced CVD as Active Layers in Chemical Gas Sensors. *Thin Solid Films* **1998,** *323* (1), 291-295.

(21) Yea, B.; Sasaki, H.; Osaki, T.; Sugahara, K.; Konishi, R., Investigation of Substrate-Dependent Characteristics of SnO_2 Thin Films with Hall Effect, X-Ray Diffraction, X-Ray Photoelectron Spectroscopy and Atomic Force Microscopy Measurements. *Jpn. J. Appl. Phys.* **1999,** *38* (4R), 2103.

(22) Themlin, J.-M.; Chtaïb, M.; Henrard, L.; Lambin, P.; Darville, J.; Gilles, J.-M., Characterization of Tin Oxides by X-Ray-Photoemission Spectroscopy. *Phys. Rev. B* **1992,** *46* (4), 2460.

RSC Advances Accepted Manuscript

(23) Andreazza, P.; Andreazza-Vignolle, C.; Kante, I.; Devers, T.; Levesque, A.; Allam, L., Buffer Layer Effect in Nanostructured Tin Electrodeposition on Insulating and Conducting Substrates. *Prog. Solid State Chem.* **2005,** *33* (2), 299-308.

(24) Deshpande, V.; Sirdeshmukh, D., Thermal Expansion of Tetragonal Tin. *Acta Crystallogr.* **1961,** *14* (4), 355-356.

(25) Dai, Z. R.; Pan, Z. W.; Wang, Z. L., Growth and Structure Evolution of Novel Tin Oxide Diskettes. *J. Am. Chem. Soc.* **2002,** *124* (29), 8673-8680.

(26) Liu, Q.; Liang, L.; Cao, H.; Luo, H.; Zhang, H.; Li, J.; Li, X.; Deng, F., Tunable Crystallographic Grain Orientation and Raman Fingerprints of Polycrystalline SnO Thin Films. *J. Mater. Chem. C* **2015,** *3* (5), 1077-1081.

(27) Choi, K.-S., Shape Control of Inorganic Materials Via Electrodeposition. *Dalton Trans.* **2008,** (40), 5432-5438.

(28) López, C. M.; Choi, K.-S., Electrochemical Synthesis of Dendritic Zinc Films Composed of Systematically Varying Motif Crystals. *Langmuir* **2006,** *22* (25), 10625-10629.

(29) Boggs, W.; Trozzo, P.; Pellissier, G., The Oxidation of Tin Ii. The Morphology and Mode of Growth of Oxide Films on Pure Tin. *J. Electrochem. Soc.* **1961,** *108* (1), 13-24.

(30) Greve, D. W., *Field Effect Devices and Applications: Devices for Portable, Low-Power, and Imaging Systems*. Prentice-Hall, Inc.: **1998**.

(31) Bardeen, J., Surface States and Rectification at a Metal Semi-Conductor Contact. In *Electronic Structure of Metal-Semiconductor Contacts*, Springer: 1990; pp 63-73.

RSC Advances Accepted Manuscript

(32) Pan, X.; Fu, L., Oxidation and Phase Transitions of Epitaxial Tin Oxide Thin Films on (012)(1̄012) Sapphire. *J. Appl. Phys.* **2001,** *89* (11).

(33) Gauzzi, F.; Verdini, B.; Maddalena, A.; Principi, G., X-Ray Diffraction and Mössbauer Analyses of SnO Disproportionation Products. *Inorg. Chim. Acta* **1985,** *104* (1), 1-7.

(34) Zhong, C.-W.; Lin, H.-C.; Tsai, J. R.; Liu, K.-C.; Huang, T. Y., Impact of Gate Dielectrics and Oxygen Annealing on Tin-Oxide Thin-Film Transistors. Jp. J. Appl. Phys. **2016**, 55, 04EG02.

(35) U, M.; Han, Y.-J.; Song, S.-H.; Cho, I.-T.; Lee, J.-H.; Kwon, H.-I. High Performance P-type SnO Thin Film Transitors with SiO_x Gate Insulator Deposited by Low-Temperature PECVD Method. J. Semicond. Technol. Sci., **2014**, 14(5), 666-672.

(36) Fortunato, E.; Martins, R., Where Science Fiction Meets Reality? With Oxide Semiconductors! *Phys. Status Solidi RRL* **2011,** *5* (9), 336-339.

(37) Hsu, P.-C.; Chen, W.-C.; Tsai, Y.-T.; Kung, Y.-C.; Chang, C.-H.; Hsu, C.-J.; Wu, C.-C.; Hsieh, H.-H., Fabrication of P-Type Sno Thin-Film Transistors by Sputtering with Practical Metal Electrodes. *Jpn. J. Appl. Phys.* **2013,** *52* (5S1), 05DC07.

(38) Nomura, K.; Kamiya, T.; Hosono, H., Ambipolar Oxide Thin-Film Transistor. *Adv. Mater.* **2011,** *23* (30), 3431-3434.

RSC Advances Accepted Manuscript

Table of Contents Graphic

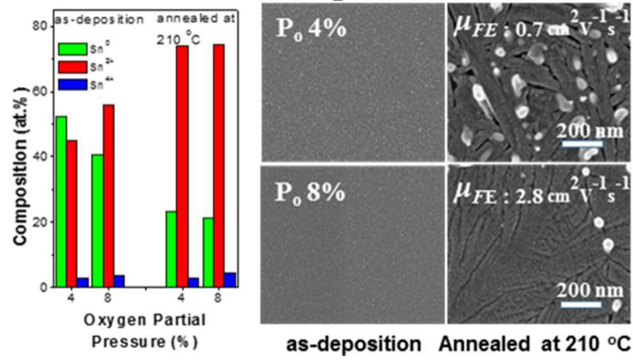

RSC Advances Accepted Manuscript